

The Oxidation of Silver by Atomic Oxygen

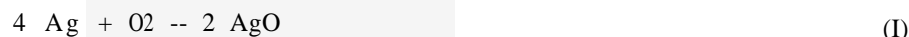
Abstract An improved model for the atomic oxygen oxidation of silver is presented. The transport of oxygen through the oxide layer is modelled using two transport mechanisms, namely gas flow through micro-pores and Fickian diffusion. Both processes exhibit parabolic growth. The interfacial reaction between oxygen and silver is taken as linear, resulting in a linear-parabolic oxidation with flux and time. The model results in a low-temperature oxidation by gas flow while at higher temperature the diffusion mechanism controls the kinetics of the oxidation. Flaking and spalling of the oxide layer is introduced in the model. This flaking behaviour of the oxide results in a linear dependence between the thickness reduction of silver and the fluence of the atomic oxygen. Predictions of the thickness loss of silver are made as a function of orbital parameters, like time of the year, inclination angle, solar activity and altitude. These calculations show that silver should not be used when exposed to atomic oxygen. Also so-called protection layers on silver are not always 100% protective. The amount of silver oxidised under the protective layer is usually much greater than the defects in the protection layers.

1. Introduction

Materials for use in future space applications in low earth orbit and exposed to the hostile combination of atomic oxygen and thermal cycling have to be screened for their susceptibility to withstand this environment over very long periods. From Space Shuttle launches a few measurements are available for some materials over test periods of 40 hours.¹ The test periods might be extended using free fliers. Real-life testing on board spacecraft for longer duration is however not practical. Accelerated testing on the ground in a controlled environment is of the utmost importance to be able to predict the behaviour of materials under atomic oxygen conditions.

One of the difficulties of laboratory simulation is translation of the test results to the real space conditions. To obtain a reasonable test duration, acceleration times of a factor 1000 are often necessary. Test environmental factors like specimen temperature, atomic-oxygen flux etc. are often held constant during the test. Also reactive gaseous states hardly equivalent to atomic oxygen are used, since an atomic oxygen source with the right parameters is not yet available.

The equilibrium electrode potential of silver is +0.799 V. This value is only 0.01 V more negative than the equilibrium potential of an oxygen electrode in natural environments. Then by definition silver is not regarded as a noble metal, because it can still be thermodynamically oxidised by atmospheric oxygen at normal temperatures. At standard temperatures and pressures (STP), the thermodynamical equilibrium of



lies as will be calculated at the right-hand side of the chemical reaction. The thermo-

Nomenclature

A	= surface area (cm ²)	n_2	= density of O-atoms at bottom of pore (at/cm ³)
A_p	= geomagnetic index	P	= porosity (%)
C	= conversion factor atoms/cm ³ to cm ³ silver	P_c	= Clausing factor
C_1	= aperture conductance (cm ³ /s)	P_{O_2}	= partial pressure of oxygen (atm)
D	= diffusion constant (cm ² /s)	Q	= activation energy (cal/mol)
dy/dt	= oxide growth rate (cm/s)	R	= gas constant (1.987 cal/mol/K)
E	= energy of oxygen atoms or ions (eV)	R_h	= hydraulic radius of pore (cm)
E_{th}	= energy threshold for sputtering (eV)	T	= temperature (K)
$F_{10.7}$	= solar flux at radio wavelength 10.7 cm (10 ⁻²² W/m ² /Hz)	t	= time (s)
F_1	= oxygen flux due to gas flow (at/cm ³ /s)	v	= velocity (cm/s)
F_2	= oxygen flux due to diffusion (at/cm ³ /s)	v_o	= most probable speed of atoms (cm/s)
F_3	= oxide flux due to oxidation (at/cm ³ /s)	v_1	= velocity of O-atoms at aperture of pore (cm/s)
F_{12}	= oxygen flux from aperture to bottom of pore	v_2	= velocity of O-atoms at bottom of pore (cm/s)
F_{21}	= oxygen flux from bottom to aperture of pore	w	= pre-constant in aperture equation
Fl	= fluence of o-atoms (at/cm ²)	x_{red}	= thickness reduction of base metal (cm)
H	= perimeter of pore (cm)	y	= oxide thickness (cm)
J	= sputtering yield (at/atom)	ΔG	= free enthalpy (kcal/mol)
K	= oxidation reaction constant (cm ² /s)	ΔH	= enthalpy (kcal/mol)
k	= Boltzmann constant (R/N_{av} cal/K)	ΔS	= entropy (cal/K/mol)
L	= pore length (cm)	$\Delta(\Delta G)$	= free enthalpy difference of reaction (kcal/mol)
m	= mass of o-atoms (g)	$\Delta(\Delta H)$	= enthalpy difference of reaction (kcal/mol)
N_{av}	= Avogadro's number (6.02217×10^{23} /mol)	$\Delta(\Delta S)$	= entropy difference of reaction (cal/mol/K)
N_p	= number of pores per cm ²	ϕ	= flux (at/cm ² /s)
n	= density of O-atoms (at/cm ³)	σ	= cross section of O-atom (cm ²)
η	= density of O-atoms at aperture of pore (at/cm ³)	Ω_{eff}	= effective volume ratio oxide/metal
		Ω_{th}	= theoretical volume ratio oxide/metal

dynamic values ΔH and ΔS for Ag, O_2 , Ag_2O and Ag_2O_2 are given in Table 1.

The direction of the chemical reaction is given by the sign of the free enthalpy of the reaction. The free enthalpy change $\Delta(\Delta G)$ of the reaction is written as

$$\Delta(\Delta G) = \Delta(\Delta H) - T\{\Delta(\Delta S) + R \ln P_{O_2}\} \quad (2)$$

where $A(A..)$ means $\Delta_{left} - \Delta_{right}$.

The free enthalpy change of reaction 1 is calculated to be -4445 cal/mol at a partial oxygen pressure of 0.2 atm. and temperature of 298 K. Since this is a negative value, the reaction proceeds towards Ag_2O .

Another possible oxidation reaction between silver and oxygen is



Calculating the thermodynamical equilibrium at STP, one finds that reaction 3 cannot proceed to the right-hand side, which means that under the given conditions AgO is not a stable oxide. The calculated free enthalpy change of reaction 3 also at a partial oxygen pressure of 0.2 atm. is +7473 cal/mol.

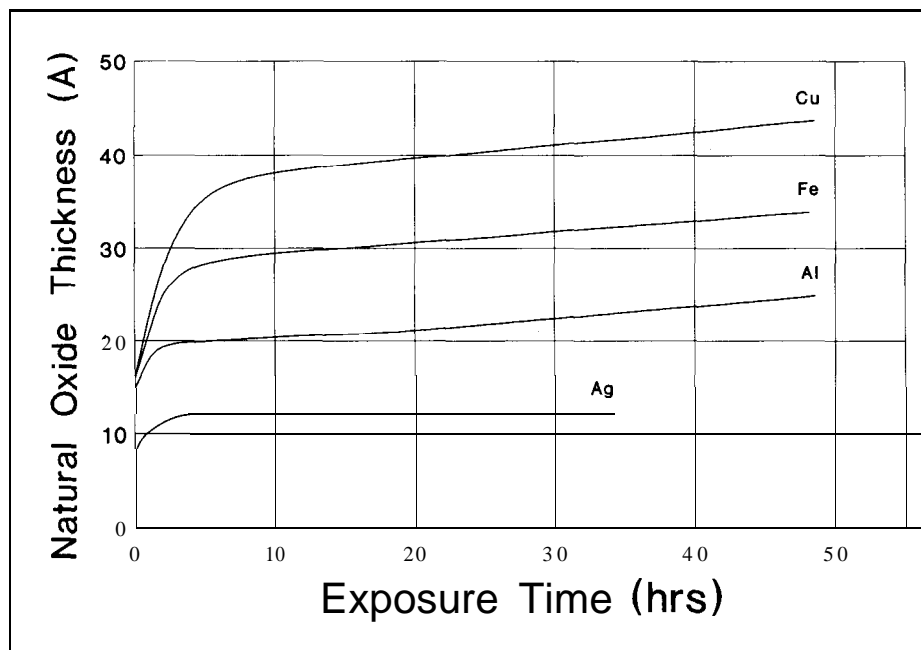
The situation is drastically changed when O-atoms instead of O_2 molecules are involved in the oxidation reaction with silver. Both oxide types are now stable even at very low pressures and also AgO is more stable than Ag_2O . It is then thermodynamically possible to oxidise Ag_2O to AgO , which was impossible with O_2 molecules.

The naturally occurring oxide thickness of Ag_2O on silver exposed to the natural oxygen environment is in the range 10 to 20 Å. The oxide thickness of various metals at room temperature is illustrated in Figure 1. The curves in Figure 1 are not to be taken as accurate as displayed. They give only the order of magnitude of the natural oxide thickness found. As noticed the curves tend to reach an asymptotic value.

Many theoretical descriptions of oxide growth are available. The outcome of these theories depends on the assumptions made for the oxidation process. The way to proceed in order to explain the oxide growth is to match the observations from experiments with these theories. If one of these theories is found to match, one can say that the basis on which this theory is founded is the same as for the oxidation of the particular gas/metal system. This means that for the explanation of the oxidation growth

Table 1. Enthalpy ΔH and entropy ΔS of the various substances present in the oxidation of silver'

	ΔH (at RT) (kcal/mol)	ΔS cal/K/mol
Ag	0	10.17
Ag_2O	-7.42	29.0
Ag_2O_2	-5.8	28.0
O_2	0	49.003
0	59.553	38.467



2. Determination Of growth model

Figure 1. Thickness of oxide formed on various metals at room temperature'

rate one always starts with observations and from that point on the applicable theory explains the oxidation mechanism.

Some observations crucial to the explanation of the oxidation mechanism are listed below:⁴

- (1) At constant temperature the oxide growth is parabolic with time.
- (2) The oxidation process is temperature dependent.
- (3) The oxidation also occurs at a significant rate at room temperature.
- (4) The oxide layer shows heavy flaking; typical thickness of a flake is 0.5 μm (see Fig. 2).
- (5) Above 100°C the oxide type is different from the one below that temperature.
- (6) The energy of the oxidising atoms is of minor importance when the oxide growth is related to the number of oxygen atoms per unit surface and time arriving at the surface.
- (7) The volume ratio oxide/metal is around 2.
- (8) After removal of the oxide layer sometimes a second strong adherent oxide layer is found (see Fig. 3).

The oxide growth model for silver exposed to energetic atomic oxygen has to take the above points into account.

Observation 1, the parabolic oxide growth, is important, because it rules out some oxidation growth models sometimes found in gas/metal systems (e.g. linear, cubic, logarithmic, inverse logarithmic growth, Fig. 4). The way to establish the oxide growth type is to plot the oxide growth measurements using the general formula:

$$y^p = \text{constant } t \quad (4)$$

Equation 4 has to be used with some caution, since it does not cover the logarithmic and inverse logarithmic growth. Plotting the data in a double logarithmic fashion, a straight line should be found where the slope (1/p in Equation 4 determines the oxidation process. A deviation from this straight line could mean that Equation 4 is not applicable or that an additional mechanism is operational. Three series of oxidation results from Reference 4 are plotted using the logarithmic form of Equation 4 and the results are depicted in Figure 5.

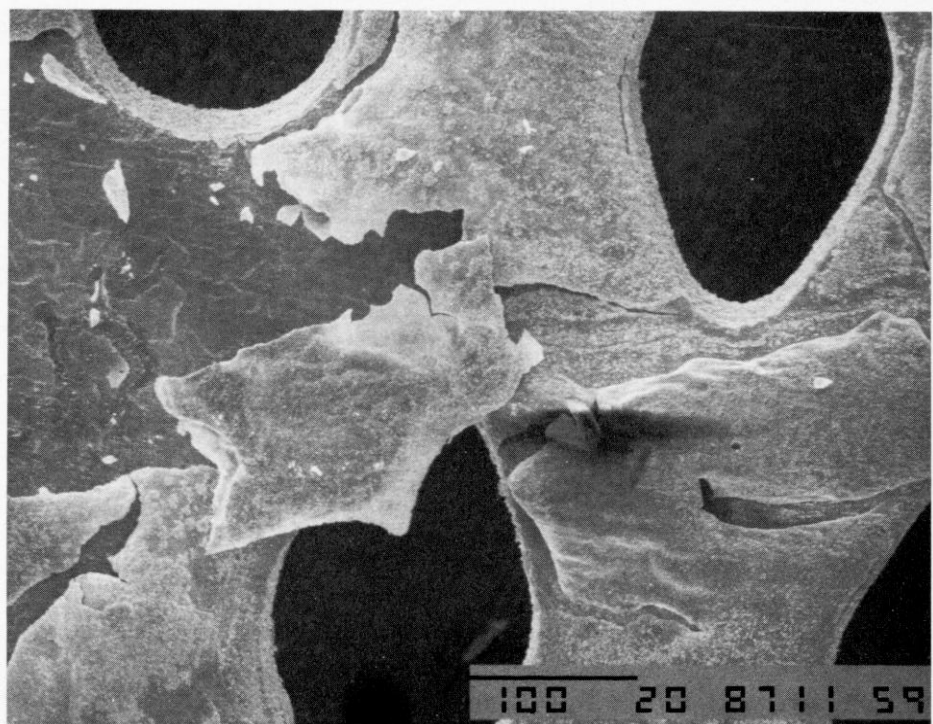


Figure 2. Oxidised silver surface after exposure to atomic oxygen in space (STS-8), showing severe flaking of the oxide

Least-square analysis of the slopes in Figure 5 indicates a value of p between 2 and 2.3. A small deviation from a straight line is found at short exposure time. The slope in that region is somewhat higher, giving a lower value for p . The value for p is close enough to 2 to assign $p = 2$. (In Reference 4 the actual value determined from the least-squares analysis is used throughout the calculations.)

If $p = 2$, one says that the oxidation process is parabolic. Only a few physical processes can explain parabolic growth of an oxide layer. One of the well-known processes is a diffusion-controlled oxidation where the oxidiser or the metal ions diffuse through the oxide layer governed by a Fickian transport mechanism. The diffusion rate of a gas through a layer is inversely proportional to the thickness of that layer. Using this behaviour in oxidation theory one finds that the oxidation-growth rate is inversely proportional to the local thickness of the oxide layer. Integration of the diffusion-controlled oxide-growth rate yields the desired factor $p = 2$ for the oxide growth.

$$\frac{dy}{dt} = \frac{K}{y} \quad \rightarrow \quad y^2 = K.t \quad (5)$$

Item 2 on the observation list, the observed temperature dependence of the oxidation, also favours a diffusion-controlled mechanism. The effect of temperature on the rate of oxidation is directly related to the temperature coefficients of the reaction rate constant in the initial stage of oxide-film growth and of the diffusion coefficient in the presence of a protective oxide layer. It has been established that the chemical reaction rate constant and the diffusion coefficient increase exponentially with the temperature and we may expect that the oxidation rate will also vary exponentially with the temperature. Usually the oxidation rate is then expressed by the following Arrhenius equation:

$$\frac{dy}{dt} = a \cdot \exp\left(-\frac{Q}{RT}\right) \quad (6)$$

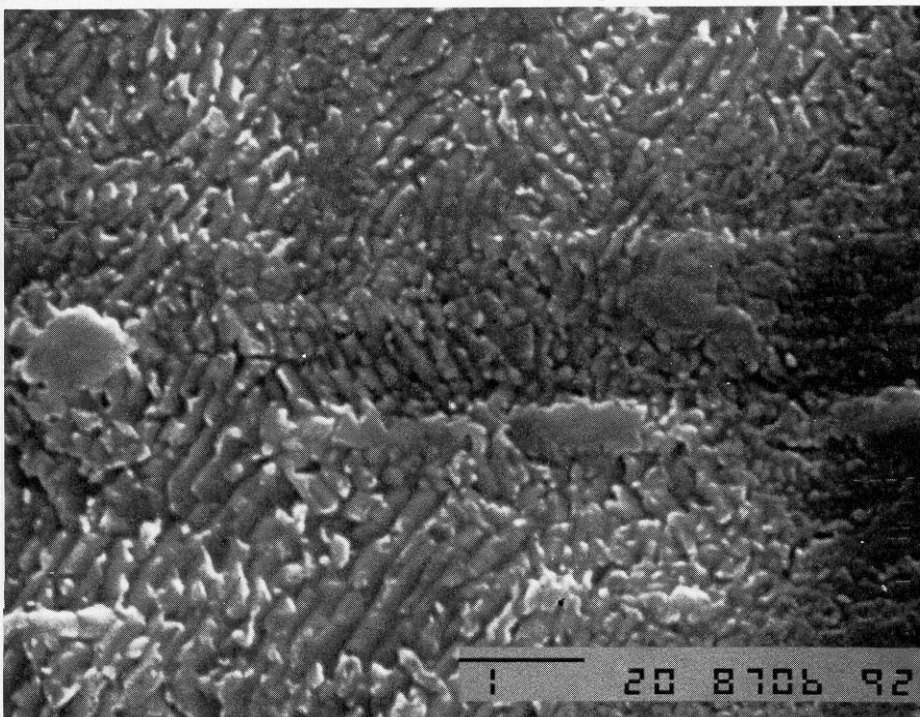


Figure 3. Second oxide layer visible after the primary oxide layer has been removed. This oxide layer has an amorphous structure

Item 3 of the observation list, the relatively high oxidation rate at room temperature, reduces however the possibility of a diffusional transport mechanism through the oxide layer. As the diffusion is a temperature-controlled process, the observation of a substantial amount of oxidation at room temperature indicates a different oxidation process or at least a parallel process capable of oxidising the metal in a parabolic manner and operational at low temperatures. The process responsible for the low-temperature oxidation is known as gas flow through micro-pores.⁵ As argued in Reference 4, this transport mechanism is also of the parabolic type as the flow resistance of a gas through a micro-pore is inversely proportional to the length of that micro-pore. Simply by observing the oxidation growth rate of a metal, one cannot distinguish the diffusional transport from the gas-flow transport. The advantage and at the same time the weakness of a gas-flow transport mechanism is its weak temperature dependence. It cannot explain the observed temperature relation found in the experiments and it violates item 2 in the observation list, but it is still operational at very low temperatures.

From the above arguments it is clear that in order to explain items 1, 2 and 3 of the observation list, both transport processes should work in parallel. Some of the oxidising atoms are transported through the oxide layer via a diffusional mechanism while another part of the oxidiser is transported via a gas-flow process. At relatively high temperature, the diffusional mechanism is dominant, while at low temperatures the gas flow through micro-pores is the important process. Items 4 and 7 of the observation list, the appearance of flaking of the oxide layer, indicate stresses in the oxide layer. These stresses result from the twofold increase in volume of the oxide reaction layer, which as it increases in thickness will be subjected to a progressive increase in compressive stress. The oxide-to-metal volume ratio of two is not so high that large stresses can develop and indicates that the formed silver oxide has a very low strength. As soon the oxide layer reaches a thickness of $0.5 \mu\text{m}$, the internal stresses grow larger than the strength of the oxide and flaking occurs.

Item 5 of the observation list, the change in oxide type at a temperature above 100°C , tells us that any experiment simulating the atomic oxygen attack on silver should be performed at temperatures below that transition temperature. The oxide type formed below 100°C is AgO , while over 100°C Ag_2O is formed. The relatively minor role of the energy in the oxidation process can be misleading. It is customary practice in the atomic oxygen erosion treatment to relate the degradation of materials to the flux or fluence of the oxygen atoms. The energy-dependent part of the erosion process is then disguised in the given flux or fluence, since the flux is related to the square root of the energy via

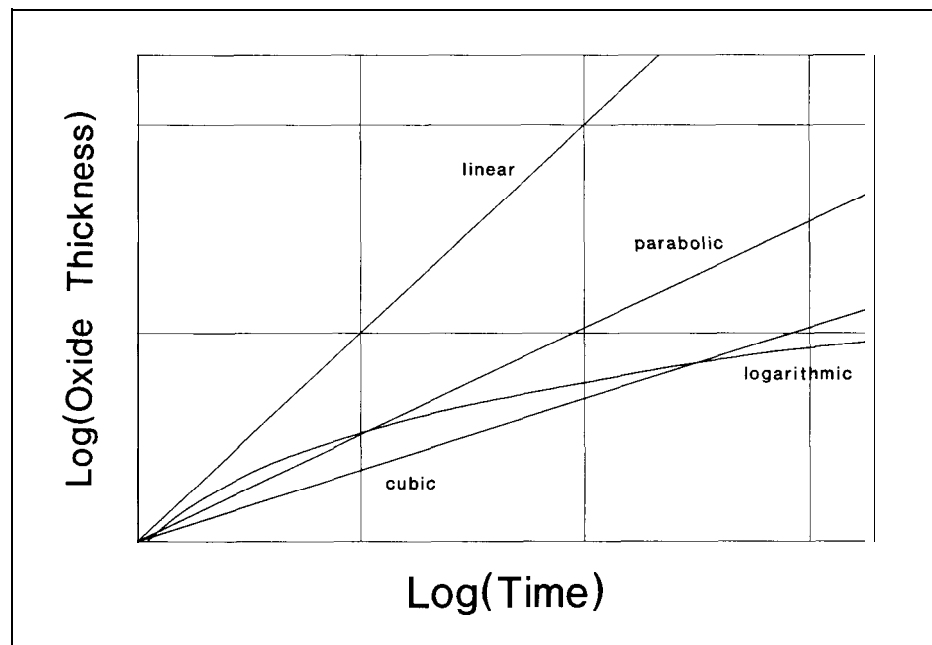


Figure 4. Double logarithmic plot of the various oxidation mechanisms

$$\phi = n.v \text{ and } E = \frac{1}{2} m.v^2 \quad (7)$$

where n is the number density of the oxygen atoms, m their mass and v their velocity. Because of the high energies sometimes used in certain experiments, a second energy-dependent process plays a part in the description of the oxide growth model. If the energy of the bombarding atoms is higher than the threshold energy for physical sputtering, oxide atoms will be removed from the oxide surface, resulting in a thinner oxide layer than oxidation attack alone would lead one to expect.

The 7th item in the observation list, the oxide/metal volume ratio, gives us an idea of the amount of void space in the oxide layer. The theoretical volume ratio of AgO is 1.6 and the observed value of 2 gives a void space of 20% over the measured oxide thickness.

The 8th item from the observation list, an adherent oxide layer on the base metal after the main oxide layer has been removed, is often observed in corrosion practice. It is usually a low-oxygen-containing oxide between the base metal and the main oxide and forms the basis for the idea that the oxidation occurs in two steps, namely $\text{Ag} \rightarrow \text{Ag}_2\text{O} \rightarrow \text{AgO}$.

The description of the rate mechanisms of the reaction between materials and oxygen known as oxidation has a very long history. The largest amount of experimental work in the science of oxidation has been carried out on the metal/oxygen system and, more recently, on semiconductor/oxygen systems. The following description of the rate factors involved in oxidation depends heavily on the formulations derived for systems of these types; however, in the general formulation no structure factors are included and consequently the approach is also applicable to non-metals under oxygen attack.

The relationship between the thickness of the oxide layer and the total duration of the exposure in most cases describes the oxidation rate. The rate of oxidation after the initial stage depends on whether the possible oxidation layer remains protective as it grows or whether it is virtually absent and nonprotective. The latter possibility is also applicable to those oxide layers that contain cracks and pores, these being taken to be nonprotective. The phenomenon of cracking of the oxide layer will be discussed later in this paragraph.

Oxidation rates are usually described in an O_2 environment using Fickian diffusion of the oxidant or metal ions through the growing oxide layer. The initial stage, when no oxide layer is present, is mainly ignored in the case of protective oxides. Oxidation

3. Description Of the oxidation process

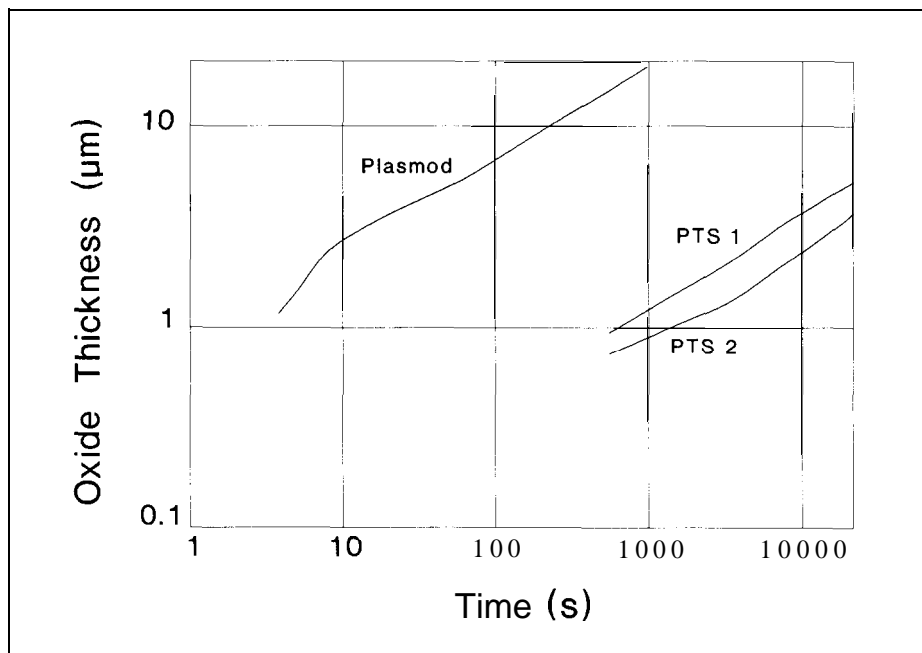


Figure 5. Double logarithmic plot of PLASMOD data and PTS-Germany data'

rates obtained with these assumptions diminish with time, and parabolic, cubic or logarithmic growth is predicted.

Revision of these thermal growth models is necessary if one is to explain the increased oxidation growth rates observed under energetic atomic oxygen bombardment. The increased growth rate is partly a consequence of the fact that atomic oxygen is much more reactive than the O₂ molecules and partly due to the penetration of the energetic oxygen atoms below the surface of the oxide layer.⁴ Another enhancement is due to a different transport mechanism through the oxide layer. Fickian diffusion at the low temperatures found in the space environment is much too slow to account for the increased diffusion rates.

In order to account for the energetic oxygen environment, consideration must be given to the simultaneous occurrence of oxidation and sputtering processes at the sample. To obtain the correct growth rate in the presence of sputtering whenever high-energy neutrals or ions are involved, one has to subtract the sputter rate from the steady-state oxidation growth rate. Following Greiner,⁶ we write:

$$\frac{dy}{dt} = \left(\frac{dy}{dt}\right)_{\text{oxidation}} - \left(\frac{dy}{dt}\right)_{\text{sputtering}} \quad (8)$$

The two rate processes will be treated separately: first, the steady-state oxidation growth rate.

3.1 Oxidation of silver by two parallel transport mechanisms

The physics of gas flow through a micro-pore depends upon the relationship between the mean free path for molecule collisions and the dimensions of the pore. At very low pressures, wall collisions are more frequent than collisions with other molecules. This is termed the free-molecular regime. At higher pressures, where the collisions with other molecules are frequent, the flow of an individual molecule is determined by the neighbouring molecules and their motion. This regime is called viscous flow.

The pressure regime which marks the gradual transition between viscous flow and free molecular flow occurs when the mean free path is comparable to the diameter of the pore. The diameter of a micro-pore in the silver oxide layer is in the nm to μm range and a safe estimate is 100 nm.

The mean free path is given as:

$$\Lambda = (\sqrt{2} \cdot n \cdot \sigma)^{-1} \quad (9)$$

where n = density of atoms per cm³ and σ = effective molecular cross section.

The cross section σ is related to the molecular diameter d as

$$\sigma = \frac{1}{4} \cdot \pi \cdot d^2 \quad (10)$$

The atomic volume of O-atoms is given as $V_{\text{oxygen}} = 14 \text{ \AA}^3$. The diameter of an O-atom, assumed spherical, is then $d = 3 \text{ \AA}$ and with a density of O-atoms in low earth orbit of approximately 10^8 atoms/cm^3 , the mean free path is ca. $10^7 \mu\text{m}$.

In our case the mean free path is considerably greater than the diameter of the pore, and free molecular flow is expected. The number of atoms flowing through a pore is determined by the conductance of the pore, which is a measure of its ability to transport gas and is expressed in units per volume per unit time.

There are two aspects which determine the conductance of a pore:

- (1) the rate at which molecules enter the pore, and
- (2) the probability that these molecules are transmitted through the system.

The first item depends upon the area of the entrance aperture, while the latter is determined by the series of reflections from the walls which result in the molecule eventually being transmitted through the pore or reflected back. The volume of gas transmitted from one side of the aperture to the other per unit time (the aperture conductance) is

$$C_1 = w \cdot v_1 \cdot A \quad (11)$$

where the pre-constant w depends on the gas statistics and v_1 and A are respectively the mean velocity of the gas and the surface of the aperture. For a gas described by Maxwell-Boltzmann statistics, the w -factor is $1/4$, while for a gas having directional flow $w = 1$.

The conductance of a tube is given by the Clausing factor, which is the possibility that a gas atom is transmitted through a tube. Atoms arriving at the opening of a tube strike the wall of this tube after a certain flow length. At this point, the atoms are reflected in a random direction; every atom has a chance of being reflected forwards or backwards.

The Clausing factor P_c of a tube of length L , a cross section A and perimeter H is approximated by⁷

$$P_c = [1 + (3/16) L \cdot H/A]^{-1} \quad (12)$$

The gas flow from 1 to 2 (see Fig. 6), if the base metal is absent and replaced by a perfect vacuum and if there is directional flow of the gas atoms, is

$$F_{12} = n_1 \cdot v_1 \cdot A \cdot P_c \quad (13)$$

where

n_1 = density of the gas atoms at point 1

v_1 = velocity of gas atoms at point 1.

The backflow in the tube from 2 to 1, if at point 1 a perfect vacuum is present and at point 2 the gas atoms move in random directions described by Maxwell-Boltzmann statistics, is given as

$$F_{21} = 1/4 \cdot n_2 \cdot v_2 \cdot A \cdot P_c \quad (14)$$

The net flow in the tube is then given by the difference between the flow from 1 to 2 and 2 to 1. If N_p is the number of pores per unit area, then the net flow per unit area is

$$F_1 = N_p \cdot A \cdot P_c (n_1 \cdot v_1 - 1/4 \cdot n_2 \cdot v_2) \quad (15)$$

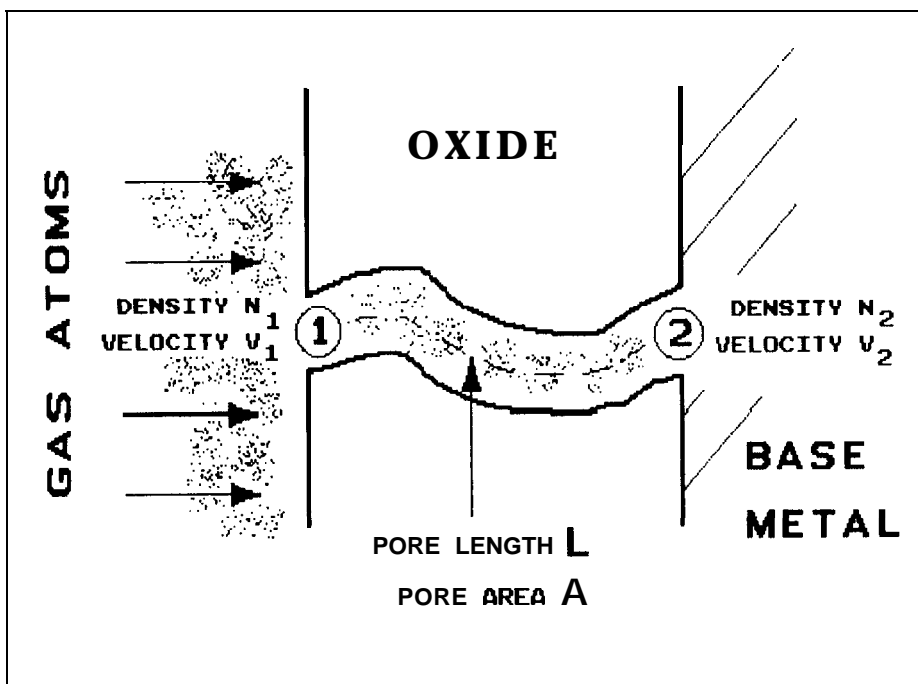


Figure 6. Model of oxide layer with pore

Only $N_p \cdot A \text{ cm}^2$ per cm^2 surface area is used for the flow of atoms through micro-pores. The remaining surface does not contribute to the flow, since no pores are present there. The atoms reaching this part of the surface diffuse through the oxide layer according to a normal Fickian transport mechanism.

At the oxide surface exposed to the oxygen atoms, the density of these atoms is n_1 and their velocity v_1 . At the oxide/metal interface, the density of oxygen atoms is n_2 and their velocity v_2 is dictated by the temperature of the base metal. At impact on the outer oxide surface, the oxygen atoms lose energy and travel through the oxide at the reduced speed v_2 . This speed reduction causes an accumulation of oxygen atoms at the surface and consequently an increase in density, which is proportional to the ratio of the velocities, written $n_1 \cdot v_1 / v_2$.

The flux of atoms through the oxide layer due to diffusion is then given as

$$F_2 = \frac{D(1-N_p \cdot A)}{Y} (n_1 \cdot v_1 / v_2 - \frac{1}{4} n_2) \quad (16)$$

where

D = diffusion coefficient with a temperature dependence

$$D = D_0 \exp(-Q_{\text{diff}}/RT)$$

y = oxide thickness

At the oxide/metal interface, the oxygen atoms react with the base metal and form the oxide. Such interface reactions are usually linear, with an oxide flux of

$$F_3 = K \cdot \frac{1}{4} n_2 \quad (17)$$

where

K = oxidation constant with a temperature dependence

$$K = K_0 \exp(-Q_{\text{ox}}/RT)$$

For a steady-state situation, the total oxygen flux from the gas flow through the micro-pores, F_1 , and from the Fickian diffusion through the remaining oxide layer, F_2 , must be equal to the oxide flux F_3 produced by the oxidation:

$$F_1 + F_2 = F_3 \quad (18)$$

Substituting Equations 15, 16 and 17 in Equation 18 enables us to eliminate the generally unknown quantity n_2 , giving

$$n_2 = \frac{4n_1 \left(N_p \cdot A \cdot P_c \cdot v_1 + \frac{D(1-N_p \cdot A) \cdot v_1}{y \cdot v_2} \right)}{K + N_p \cdot A \cdot P_c \cdot v_2 + \frac{D(1-N_p \cdot A)}{y}} \quad (19)$$

The unit for the oxide flux F_3 is $\text{atoms}/\text{cm}^3/\text{s}$ and is related to the oxide growth rate dy/dt via

$$\left(\frac{dy}{dt} \right)_{\text{ox}} = C \cdot \Omega_{\text{eff}} \cdot F_3 \quad (20)$$

where

C = conversion factor $\text{atoms}/\text{cm}^3 \rightarrow \text{cm}^3$ metal

$$c = \frac{\text{atomic weight}}{N_{\text{av}} \cdot \text{density}}$$

N_{av} = Avogadro's number
then $C = 1.7052 \cdot 10^{-23}$ for silver

Ω_{eff} = effective volume ratio oxide/metal

$$\Omega_{\text{eff}} = \frac{\Omega_{\text{th}}}{1 - P}$$

P = porosity = $N_p \cdot A$

Ω_{th} = theoretical volume ratio oxide/metal

$\Omega_{\text{th}} = 1.6$ for silver

The oxide growth rate can now be obtained by substituting Equations 17 and 19 in Equation 20. This result is written as

$$\left(\frac{dy}{dt}\right)_{\text{ox}} = \frac{C \cdot \Omega_{\text{eff}} \cdot K \cdot n_1 \left(N_p \cdot A \cdot P_c \cdot v_1 + \frac{D(1 - N_p \cdot A) \cdot v_1}{y \cdot v_2} \right)}{K + N_p \cdot A \cdot P_c \cdot v_2 + \frac{D(1 - N_p \cdot A)}{Y}} \quad (21)$$

Equation 21 is the master equation for oxide growth governed by the gas flow and diffusion transport mechanism through the oxide layer. At the onset of the oxidation, when no oxide layer is present on the base metal, the oxidation is linear.

To make Equation 21 accessible for comparison with experimental oxidation results, one simplification will be introduced. The actual length of the micro-pores is in general greater than the thickness of the oxide layer, but is not known. It will be assumed that the micro-pores are straight and normal to the surface. This condition is illustrated in Equation 22:

$$L = y \quad (22)$$

This assumption reduces the Clausing factor to

$$P_c = [1 + (3/8) y/R_h]^{-1} \quad (23)$$

where

R_h = hydraulic radius of the pore

$$R_h = 2AIH$$

with A = cross-sectional surface area of pore

H = cross-sectional perimeter of pore

(for circular tubes $R_h = R$)

After some algebra and the relations for Ω_{eff} and for the flux ϕ ($\phi = n_1 \cdot v_1$) have been inserted, the oxide growth equation is written as

$$\left(\frac{dy}{dt}\right)_{\text{ox}} = \frac{\frac{1.6 C \cdot K \cdot \phi}{v_2(1-P)}}{1 + \frac{K \cdot y}{\frac{P \cdot v_2 \cdot y}{1 + (3/8) \cdot y/R_h} + D(1-P)}} \quad (24)$$

Equation 24 can be readily integrated, under the condition that $y \gg R_h$, using standard methods, yielding

$$y + \frac{3K \cdot y^2}{16P \cdot R_h \cdot v_2 + 6D(1-P)} = \frac{1.6 C \cdot K \cdot Fl}{v_2(1-P)} \quad (25)$$

with

$$Fl = \text{fluence} = \int \phi \cdot dt$$

Equation 25 is a linear-parabolic equation; at small thicknesses the linear term predominates, while at large thicknesses the quadratic term controls the equation. The denominator of the quadratic term in Equation 25 consists of two parts, namely the gas-flow part and the diffusion part. By assigning one of the processes absent, one can calculate the contribution of the other process to the amount of corrosion.

If the diffusion process is absent ($D = 0$) and y is large, then

$$y^2 = \frac{8.53 P.R_h.C.Fl}{(1 - P)} \quad (26)$$

As may be noted from Equation 26, no temperature-dependent factor is present, meaning that the corrosion process due to gas flow in micro-pores is independent of the temperature (it is assumed that the pore size and the porosity are independent of the temperature).

If, in contrast to the above, the molecular flow process is absent (the Clausing factor $P_c = 0$) and y is large, then

$$y^2 = \frac{3.2 C.D.Fl}{v_2} \quad (27)$$

Equation 27 shows a temperature dependence through the diffusion coefficient D and the velocity v_2 .

Equations 26 and 27 demonstrate that at low temperature the molecular flow through the micro-pores is the dominating process, while at high temperature the diffusion through the oxide layer is the rate-controlling process.

3.2 Evaluation of the sputtering rate

The sputtering rate increases with the energy of the incoming gas species. No sputtering occurs until the energy of the incoming gas reaches the threshold energy E_{th} , which is characteristic of the particular gas/target combination. Initially the sputtering rate increases quadratically with the energy. At fairly low energies, this quadratic behaviour becomes linear.⁸ At still higher energies (1 to 5 keV, depending on the gas/target combination), the sputtering curve reaches a maximum, after which the rate decreases again. This energy dependence of the sputtering rate is indicated in Figure 7.

In the space environment, the energy of the atomic oxygen bombarding the surface is approximately 5 eV. With the test equipment used, the energy of the bombarding species is in the range of 50 to 300 eV and consequently the sputtering rate increases linearly with the energy, giving

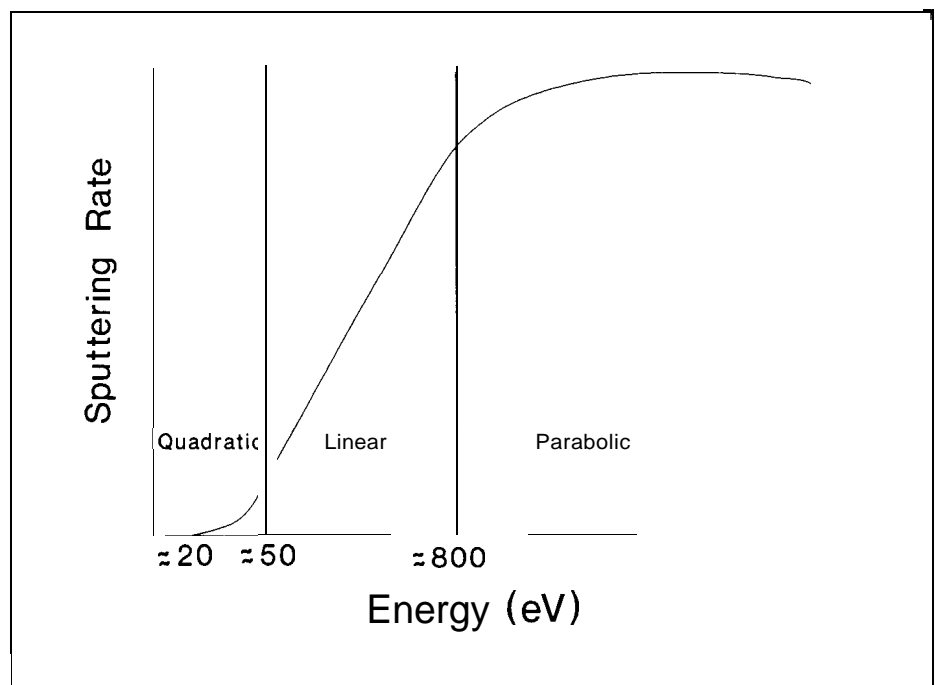


Figure 7. General shape of sputtering rate versus energy for various metals'

$$\left(\frac{dy}{dt}\right)_{sp} = J.E.\phi_i \quad (28)$$

where J is the energy-independent sputtering yield and ϕ_i is the number of incoming atoms/ions.

The total thickness change of the oxide layer due to oxidation and sputtering is then written in accordance with Equation 8 as

$$\left(\frac{dy}{dt}\right) = \left(\frac{dy}{dt}\right)_{ox}^* - J.E.\phi_i \quad (29)$$

Equation 29 is the basic equation for the calculation of the oxide growth under atomic oxygen bombardment.

If the reactive gas is atomic oxygen, the number of incoming species ϕ_i is identical to the atomic oxygen flux ϕ . If, however, the reactive gas is an oxygen plasma, the O_2^+ ions of the plasma will dissociate into two O^+ ions at collision. In this case, the oxygen flux ϕ is twice the flux of the incoming ions. At the same time, the energy of one O_2^+ ion is now shared by two O^+ ions and under momentum transfer the energy per ion is halved.

It has to be noted that a balance between sputtering and oxidation will occur when $dy/dt=0$. The growth of the oxide layer purely due to oxidation shows a linear-parabolic behaviour resulting in a diminishing oxide growth with time. The sputtering action of the incoming gas atoms is, however, linear with time. The simultaneous action of the two processes implies a limiting thickness of the oxidation layer under oxidative sputtering conditions. If the sputtering rates and the oxidation rates are equal ($dy/dt=0$), the limiting oxide thickness y_{lim} can be calculated from Equation 29. After substituting $y = y_{lim}$ and reworking Equation 29 with the condition $y \gg R_h$, we find

$$y_{lim} = \{8PR_h v_2 + 3D(1-P)\} \left\{ \frac{1.6C.\phi}{3v_2(1-P).J.E.\phi_i} \frac{1}{3K} \right\} \quad (30)$$

The fact that for high sputtering rates or for low oxidation rates a limiting oxide thickness is reached does not mean that during this stage no base metal loss occurs. At this stage, the sputtering and the oxidation are in a dynamic equilibrium. As soon as the limiting thickness is reached, any amount of oxide sputtered away from the oxygen/oxide interface is replenished by an additional oxidation at the metal/oxide interface, because after the sputtering action, the oxide layer is again smaller than the limiting thickness. After the limiting oxide thickness has been reached, the loss of base metal is proportional to the sputtering rate and will show a linear behaviour.

Secondly, dropping the temperature lowers the oxidation rate, owing to a lower diffusion rate, but does not reduce the sputtering rate. A drop in temperature under oxidative conditions accompanied by sputtering causes a smaller limiting thickness, which results in a thinner oxide layer.

The thickness change of the oxide layer is given by Equation 21, but the loss of base metal is not. The loss of base metal occurs at the metal/oxide interface where no sputtering is present. The rate of the thickness reduction of the base metal is then defined by

$$\frac{dx}{dt} = \frac{-1}{\Omega_{eff}} \frac{dy}{dt} \quad (31)$$

oxidation

The above formulation essentially treats the oxide layers as an adherent uniform scale. In practice, however, the oxide layer is not ideal. The volume of the oxide layer

* = Equation (24)

formed is generally different from that of the equivalent amount of base metal and stresses will develop. The volume ratio oxide/metal may be expected to give an indication of the magnitude and the stress (tensile or compressive).

Owing to these stresses, the surface layers will contain pores, cracks, blisters etc and will lose their protective properties. New oxide layers may be formed on the fresh metal surface, lifting the old oxide layer; subsequently this new layer may break up again, and the process repeats. Integrating this flaking process over a long time enables the loss of base metal to be approached by a straight line. This break-up mechanism is accelerated during repeated thermal cycling if the coefficient of thermal expansion of the oxide and that of the base metal are different.

The effect of flaking is introduced by defining a flaking-off thickness. Using Equation 25, we can deduct the time needed to reach a certain flaking thickness y_{flake} and, with the straight-line approximation of the base metal loss due to periodic flaking, we obtain

$$x_{red} = -z.t \quad (32)$$

with

t = time

$$z = \text{slope of the straight line } z = \frac{y_{flake}}{\Omega_{eff} \cdot t_{flake}}$$

The thickness reduction of the base metal can be written as

$$x_{red} = \frac{C.K.Fl}{1 + \frac{v_2}{16 PR_h v_2 + 6 D(1-P)}} \quad (33)$$

3.3 Constants used in the model

The same data as those in Reference 4 will be used to establish the diffusion and chemical reaction constants D_o and K_o . The values of the activation energies Q_{diff} and Q_{ox} are in the same order of magnitude and are assumed to be the same because of lack of temperature data. The sputtering constant J is also taken from Reference 4.

The other two factors, the porosity and the hydraulic radius, are measured from microsections and SEM micrographs, respectively (see Figure 8). The velocity of the oxygen atoms in the oxide layer, v_2 , is given as

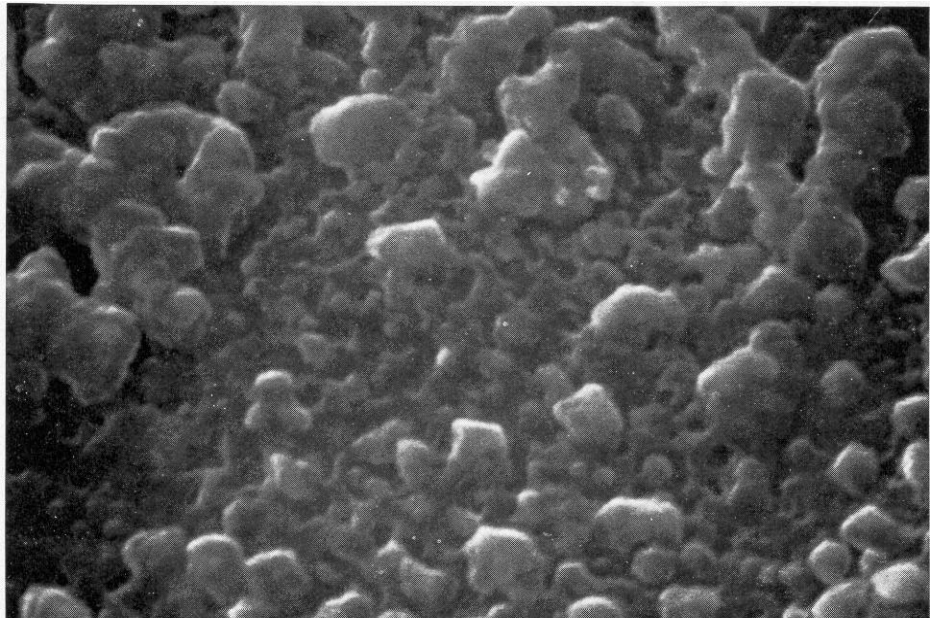


Figure 8. Atomic oxygen simulation test on

$$v_2 = \frac{2}{\sqrt{\pi}} v_o \quad (34)$$

with

$$v_o = (2 k.T/M_i)^{1/2}$$

M_i being the molecular mass, k denoting Boltzmann's constant, T the absolute temperature in Kelvin and v_o the most probable speed. The established constants are given in Table 2 and are used in the calculations.

Table 2. Constants to be used for the calculation of the oxide growth on silver under atomic-oxygen conditions

$$K = 1.134 \times 10^{15} \exp(-16194/RT)$$

$$D = 2.4593 \times 10^{10} \exp(-16194/RT)$$

$$J = 1 \times 10^{-27}$$

$$R_p = 5 \times 10^{-6} \text{ cm}$$

$$P = 0.2$$

For the computation of the oxidation of silver the results from Reference 9 will be used as the input in the calculation. In that paper ('Atomic Oxygen Fluences in Low Earth Orbit'), a systematic study was made of the atomic oxygen fluences as a function of the altitude, the solar activity, the orbital inclination and the time of year. The orbital atomic oxygen density is calculated with the aid of the MSIS-86/CIRA Neutral Thermosphere Model of Hedin.¹⁰ For consistency with the computations presented in Reference 9, the computation given here will follow the same sequence.

The ram-fluence dependence on the time of year for a circular orbit at an altitude of 400 km and with an inclination of 28° for a constant, standard solar activity ($F_{10.7} = 150$; $A_p = 15$) are calculated in Reference 9. With the aid of Equation 33 and using a flake thickness of 0.5 μm and a thermal cycle of +100/-100°C, the reduction in thickness of silver can be calculated. The result as thickness loss as a function of the time exposed in orbit is displayed in Figure 9. After one year, a silver loss of 308 μm is found. The calculation of the fluences shows two maxima around the spring and autumn equinoxes. The atomic oxygen fluences are lowest after the summer solstice in July and a second, less deep, minimum is seen in January. Over the period of a year the daily atomic oxygen fluence varies by more than 50%. This behaviour is difficult to identify in the calculated silver loss, since the attack is continuous in time and is therefore integrated over the time of exposure. Around July (month = 6) a shallow curvature is seen in Figure 9, indicating the minimum daily fluence calculated in Reference 9.

In Figure 9, the orbital inclination is given as 28°. In Reference 9, the fluences as a function of inclination are calculated for two different months at an altitude of 400 km, using the constant, standard solar activity ($F_{10.7}; A_p$) = (150; 15). The two months calculated are months 3 and 6, representing a maximum and a minimum in atomic oxygen fluence over a year.

4. Applications of the oxidation model

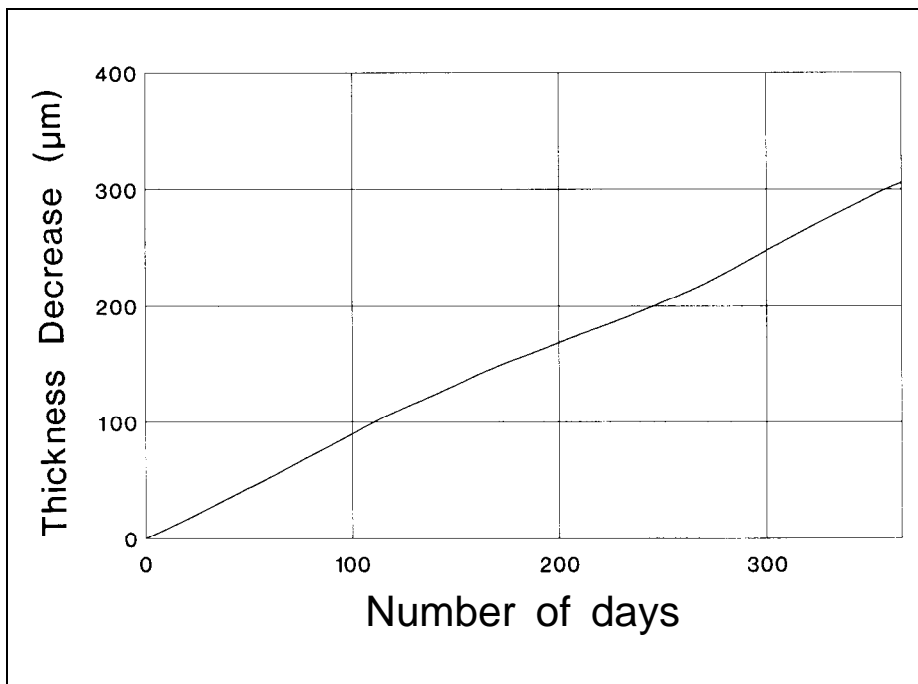


Figure 9. Calculated thickness loss of silver over a year of exposure in LEO. Incl. = 28°; Alt. = 400 km; ($F_{10.7}; A_p$) = (150; 15)

The results for the silver loss are given as a function of the time of exposure, it being assumed that with each inclination the trend of the fluence is the same for the whole year, and are presented in Figure 10. Maximum values for the loss of silver are found for small inclinations and this reflects the same trend as that found in the fluence calculation presented in Reference 9. This trend is explained by the higher atomic oxygen densities for small latitudinal values.

In Figures 9 and 10, the solar activity was taken to be the constant standard activity of $(F_{10.7}; A_p) = (150; 15)$. In Figure 11, the solar activity is varied and ranges from minimum solar activity $(F_{10.7}; A_p) = (70; 5)$ to maximum solar activity $(F_{10.7}; A_p) = (240; 25)$. The atomic oxygen ram-fluences are calculated in Reference 9 for three different altitudes, viz 200 km, 400 km and 600 km for an inclination of 28° and for month 3 of the year, representing a maximum in ram-fluence. The reduction in thickness of silver is given in micrometres per day and shows the important influence of the solar activity on the loss of silver, especially at high altitudes. The influence of the solar activity on the loss of silver is stronger, the higher the altitude. At an

Figure 10. Calculated silver reduction as a function of inclination at altitude of 400 km; $(F_{10.7}; A_p) = (150; 15)$

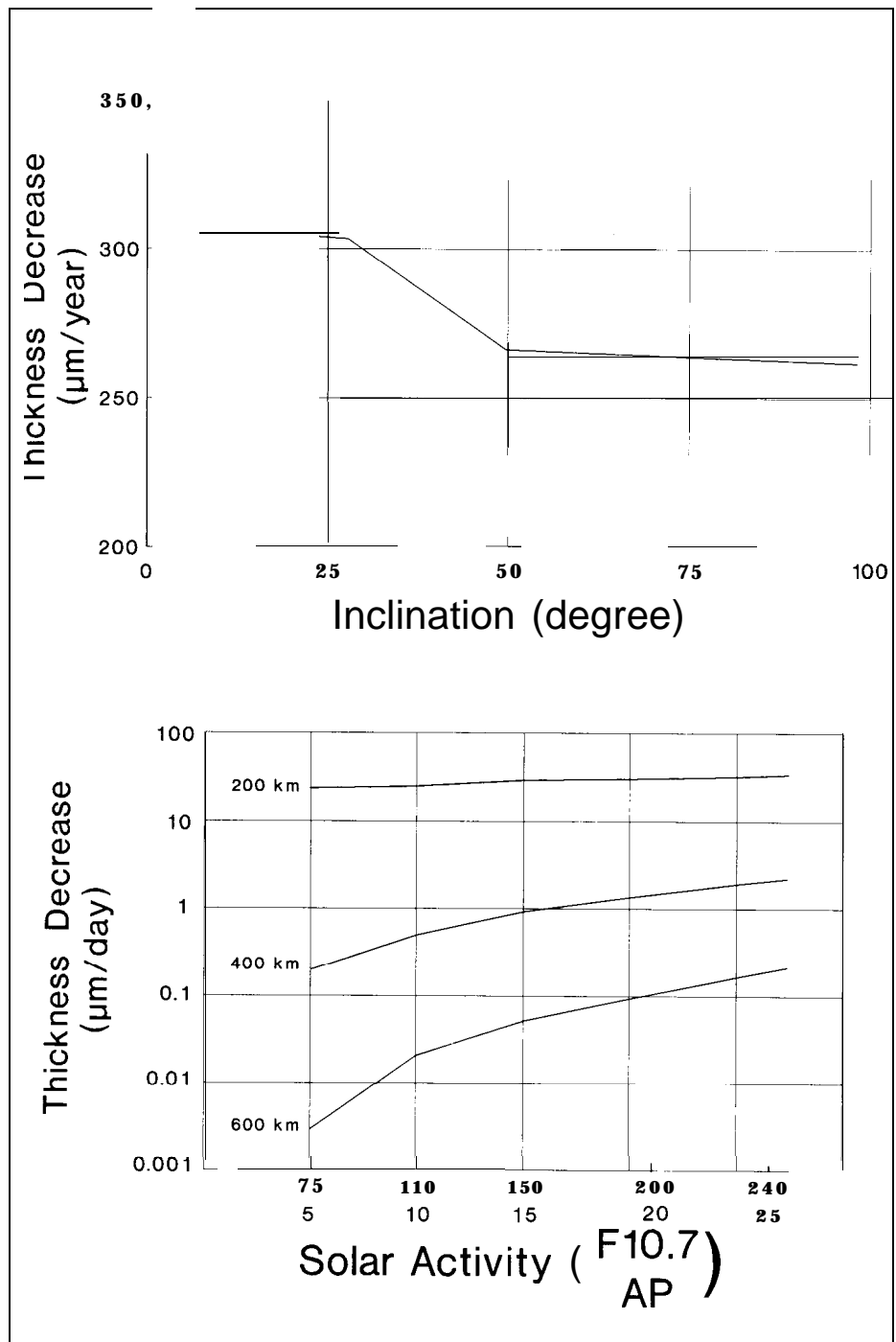


Figure 11. Calculated silver reduction per day as a function of solar activity. Incl. = 28° ; fluences for month = 3

altitude of 600 km, the difference in loss of silver between maximum and minimum solar activity is about a factor 100. The loss at maximum solar activity at an altitude of 600 km is comparable to the loss calculated for the 400 km altitude at minimum solar activity.

The last variation in the orbital environment is the dependence on the altitude. In Reference 9, the ram-fluences for heights between 200 km and 800 km are calculated for solar minimum $(F_{10.7}; A_p) = (70; 5)$, solar mean $(F_{10.7}; A_p) = (150; 15)$ and for maximum solar activity $(F_{10.7}; A_p) = (240; 25)$. In Figure 12, the loss of silver is displayed as a function of the altitude from 200 km to 800 km. The reduction of silver is given in μm per day and shows the large influence of the altitude on the loss of silver. The largest effect is found for the minimum solar activity; a factor of 10^6 is found between the lowest altitude (200 km) and the highest calculated altitude (800 km). The reduction in silver thickness as a function of altitude, plotted on a semi-logarithmic scale, exhibits an almost straight line.

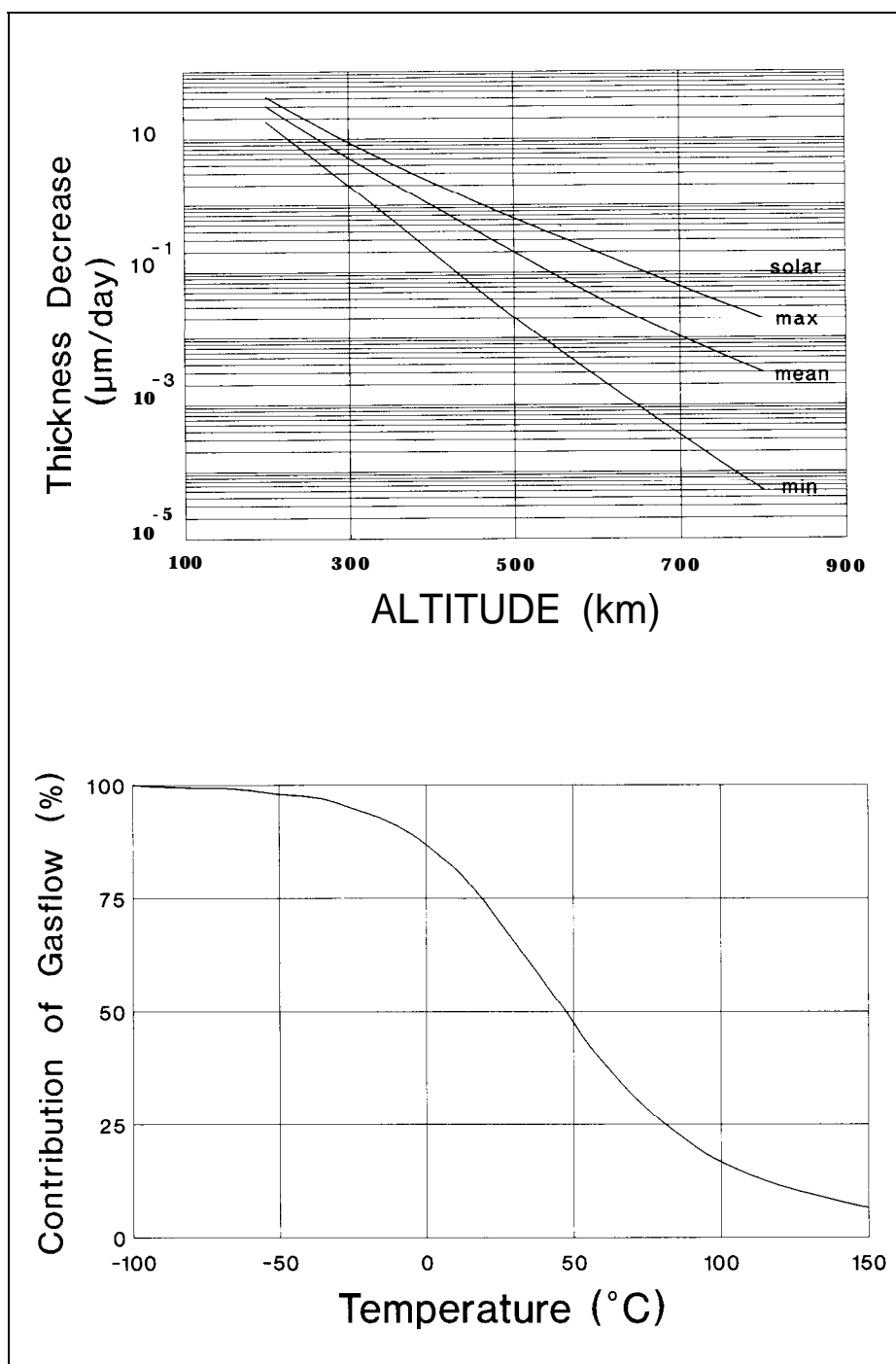


Figure 12. Calculated reduction of silver as a function of the altitude. Incl. = 28° ; fluences for month = 3

Figure 13. Calculated contribution of the gas flow to the amount of oxidation of silver exposed to atomic oxygen

5. Discussion

The major difference between the approach outlined in Reference 4 and the model presented in this paper is the transport mechanism of the oxidising gas through the oxide layer. In the approach presented in Reference 4, a single transport mechanism was assumed, viz the flow of the gas through micro-pores. The temperature dependence of the gas transport was introduced by using the well-known exponential temperature dependence of the diffusion equation. The derived oxidation equations can be regarded as a kind of hybrid solution of gas flow and diffusion. In the present model these two mechanisms are separated, which enables us to investigate the contribution of both transport mechanisms to the oxidation of silver. By considering one of the processes to be absent, the contribution of the other process can be calculated. Equations 26 and 27 are used for this purpose. In Figure 13, the gas-flow contribution to the oxidation is displayed for the temperature range -100°C to $+150^{\circ}\text{C}$. As mentioned in Section 2, the low-temperature oxidation is fully controlled by the gas flow through the micro-pores; the contribution of the diffusion transport is negligible. At around 45°C the two transport processes each contribute 50% to the amount of corrosion and only at higher temperatures is the diffusion mechanism the dominating transport process.

The higher the energy of the bombarding oxygen atoms, the deeper they penetrate into the oxide surface, after which the normal transport mechanism starts. In the present model this penetration depth is not explicitly taken into account in the equations. If the atoms follow the diffusion path, they lose their energy on impact, while the atoms following the gas-flow path keep their velocity, at least for a relatively long time, during their penetration into a micro-pore. It is believed that the two approaches are equivalent, and consequently no extra term for the penetration is included in the present model.

In general the dependence of the oxidation on the energy of the incoming oxygen atoms is minor if we assume the porosity and micro-pore size to be independent of the energy. The majority of the oxygen atoms reaching the oxide/metal interface have thermal energy. The energy carried by the oxygen atoms is converted into heat in the oxide layer and may raise the temperature of the sample slightly, thereby accelerating the oxidation process. This factor is not taken into account in the present model.

The energy of the incoming atoms starts to play a role above the sputtering threshold. The thickness of the oxide layer is then smaller than with oxidation alone. This shortens the diffusion length and increases the oxidation. At very high energy, it is possible that no oxide layer is formed, since it is immediately sputtered away by the energetic oxygen atoms. It is now possible that the metal surface itself is physically removed by the incoming oxygen atoms. None of the experiments conducted on silver⁴ showed an energy dependency, although one has to remember that the thick-

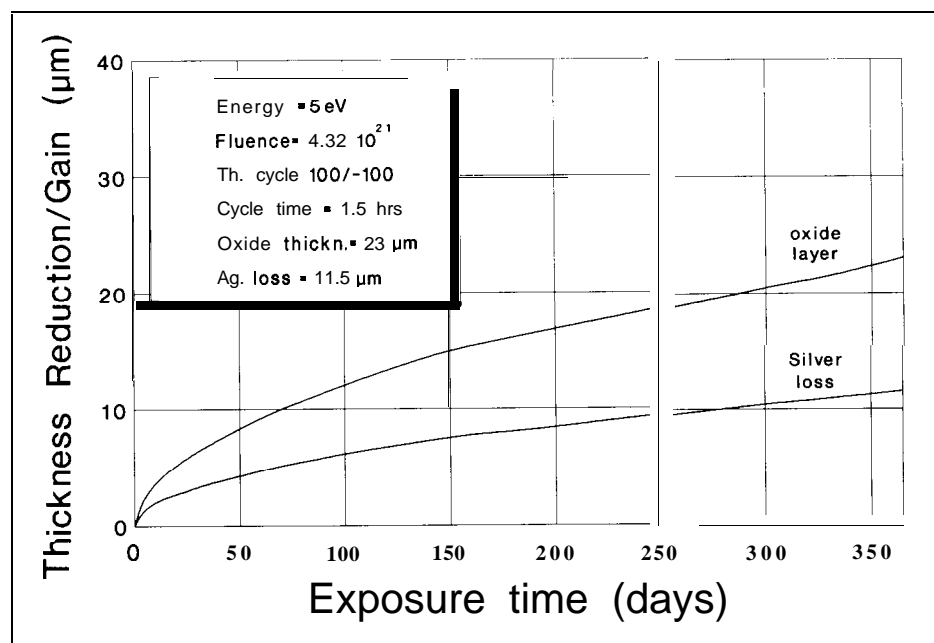


Figure 14. Calculated oxidation of silver over a period of one year of exposure in LEO if no flaking occurs. Incl. = 28° ; altitude = 400 km; $(F_{10.7}; A_p) = (150; 15)$

ness measurements on the thin oxide layers are prone to errors, which could disguise the energy effect.

In the list of observations presented in Section 2, a second oxide layer was mentioned, which was sometimes observed after removal of the outside oxide layer. On many metals with more than one type of oxide, it is often found that the oxide with the lowest oxygen content is closest to the metal surface. Examples can be found in the oxidation of copper ($\text{Cu-Cu}_2\text{O-CuO}$) and iron ($\text{Fe-Fe}_2\text{O}_3\text{-Fe}_3\text{O}_4\text{-FeO}$).

The calculation of the oxide layer thickness as a function of time can be found in the literature³ for two oxide layers, both growing in a parabolic fashion or one layer growing parabolically and the other growing linearly. This phenomenon is not only found in the oxygen reaction on certain metals, but can also be observed for example when the layers formed by the reaction between silver and sulphur ($\text{Ag-Ag}_2\text{S-AgS}$) is investigated.

The flaking and spalling of the oxide layer has a large impact on the total reduction in the thickness of silver. A flake thickness of $0.5 \mu\text{m}$ was measured on oxidised samples. In the calculation of the total amount of thickness reduction, it was assumed that the oxide layer reaching this thickness will flake off, leaving bare metal exposed to the atomic oxygen environment. This will certainly happen at some places on the exposed silver. On other parts of the surface, the oxide layer will remain on the surface because the internal stresses in the oxide layer are relieved by the flaking and spalling of the oxide. Where the oxide layer remains on the metal surface the amount of thickness reduction is less than where the oxide flakes off. The amount of thickness reduction and the thickness of the oxide layer itself can be calculated with the aid of Equation 29. The result is shown in Figure 14. After one year of exposure, a silver reduction of $11.5 \mu\text{m}$ is calculated. It can be seen that with the same orbital parameters only $11.5 \mu\text{m}$ of the base metal is lost, as opposed to $308 \mu\text{m}$ as calculated in Figure 9, where total flaking of the oxide is assumed. In real circumstances both options can occur and will result in a roughening of the surface.

Because of certain favourable properties of silver — its weldability (solar arrays) and its reflectance (mirrors) — several kinds of protection system have been tried. Such systems always involve some kind of surface layer which is intended to prevent direct contact between silver and oxygen atoms. For mirrors, only very thin transparent layers (usually stable oxides) are proposed. The drawback of such systems is their inherent brittleness with all the handling risks that this involves.

For silver parts used as structural members, protection systems ranging from polymers to gold layers have been proposed. Because of the strong interaction between silver and atomic oxygen these protection layer have to be almost perfect. Small defects, from whatever cause (manufacturing, handling, stressing etc.), cannot be permitted.

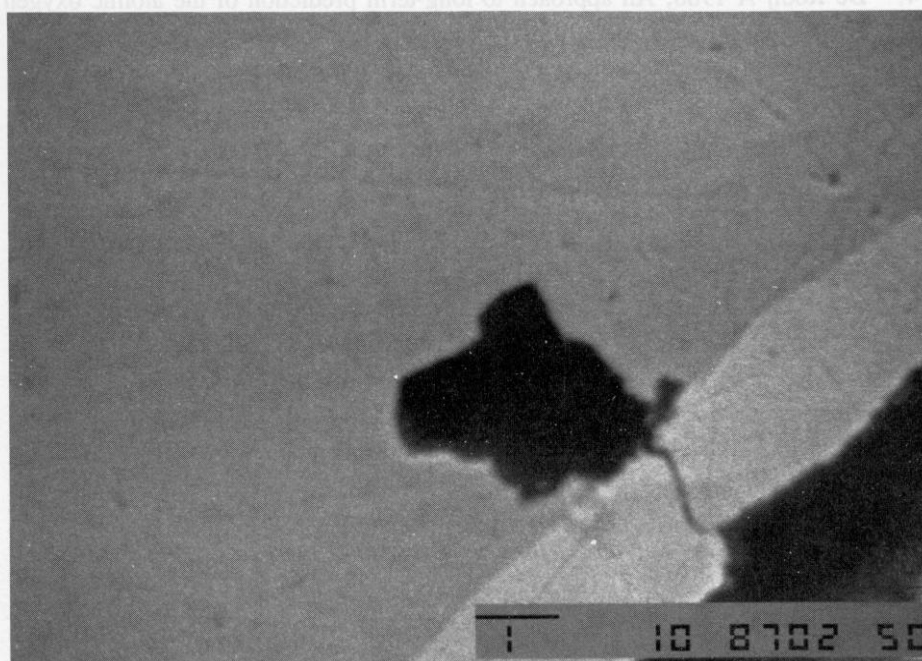


Figure 15. Microsection to highlight defect in goldplating. During exposure in an oxygen plasma the silver was oxidised through the defect

An example of a protection system investigated as part of the Space Telescope Solar Array project is the gold-plating of the silver interconnectors. Only after many difficult and discouraging experiments was a gold-plating found that gave the silver satisfactory protection. During this process it was found that even through very small defects in the plating the silver under the gold-plating was severely oxidised and that the area attacked on the silver was always many times larger than the size of the defect. An example of such a defect and the effect it has on the oxidation of the underlying silver is given in Figure 15.¹¹

6. Conclusion

An improved model of the oxidation of silver under atomic-oxygen bombardment is presented. To validate the model, the same data are used as those used for the previous approach.⁴ Within the limits of these data, the two treatments give analogous results. Outside these limits, small differences are found, which are however within confidence limits. The main reason for developing the improved model is to gain a better understanding of the low-temperature oxidation found on silver and to achieve a better separation between the processes involved in the oxidation of silver under atomic-oxygen attack.

The results of the calculations are relevant to such future long-duration projects as Columbus and equivalent space projects.

It is evident that the use of bare silver must be limited to locations not exposed to the atomic oxygen present in the low earth orbit environment. At an altitude of 400 km, a typical space-station orbit, the reduction in the thickness of silver might be in the neighbourhood of 300 μm per year. Moreover, the debris produced, silver-oxide flakes, is of concern. The typical flake size is in the order of 10 to 100 μm long by 0.5 μm thick and is electrically conductive. This could become a real orbital hazard!

Acknowledgement

The author wishes to thank Mr A. Zwaal of the Materials and Processes Division, ESTEC, for some fruitful discussions during the process of preparing this paper.

References

1. De Rooij A 1985, The degradation of metal surfaces by atomic oxygen, *Proc. Third European Symposium on Spacecraft Materials in Space Environment*, ESA SP-232, pp 99-108.
2. *Handbook of Chemistry and Physics*, CRC Press.
3. Kubaschewski O & Hopkins B E 1962, *Oxidation of Metals and Alloys*, 2nd edition, Butterworths, London.
4. De Rooij A 1988, An approach to long-term prediction of the atomic oxygen effects on materials, *Proc. Fourth European Symposium on Spacecraft Materials in Space Environment*, CERT, Toulouse, France, pp 453-463.
5. Irene E A 1983, Silicon oxidation studies: a revised model for thermal oxidation, *J. Appl. Phys.* **54**(9), p. 5416.
6. Greiner J H 1971, Josephson tunneling barriers by RF sputter etching in an oxygen plasma, *J. Appl. Phys.* **42**(12), p. 5151
7. Weissler G L & Carlson R W (Eds.) 1979, *Methods of Experimental Physics*, Vacuum Physics and Technology.
8. Carter G & Colligan J S date, *Ion Bombardment in Solids, Chapter 7, Sputtering*, Heinemann Educ. Books Ltd, London, pp 310-353.
9. Drolshagen G 1988, *Atomic Oxygen Fluences in Low Earth Orbit, A Parametric Study*, Internal Estec Report, WMA/GD/AO/11.
10. Hedin A E 1987, MSIS-86 Thermospheric Model, *J. Geophys. Res.* **A5**(92), p. 4649.
11. De Rooij A 1987, *Investigation of the discoloration and ATOX resistance of gold-plated silver interconnector before and after thermal cycling*, Internal ESTEC Report, M.G.I. 1375.

Manuscript received 15 August 1989